nature catalysis

ARTICLES

https://doi.org/10.1038/s41929-021-00618-w

Analysis of the limitations in the oxygen reduction activity of transition metal oxide surfaces

Hao Li[1,4], Sara Kelly[2,4], Dan Guevarra[3], Zhenbin Wang[1], Yu Wang[3], Joel A. Haber[3], Megha Anand[1], G. T. Kasun Kalhara Gunasooriya[1], Christina Susan Abraham[1], Sudarshan Vijay[1], John M. Gregoire[3] and Jens K. Nørskov[1] ✉

The oxygen reduction reaction (ORR) is the key bottleneck in the performance of fuel cells. So far, the most active and stable electrocatalysts for the reaction are based on Pt group metals. Transition metal oxides (TMOs) constitute an alternative class of materials for achieving operational stability under oxidizing conditions. Unfortunately, TMOs are generally found to be less active than Pt. Here, we identify two reasons why it is difficult to find TMOs with a high ORR activity. The first is that TMO surfaces consistently bind oxygen atoms more weakly than transition metals do. This makes the breaking of the O–O bond rate-determining for the broad range of TMO surfaces investigated here. The second is that electric field effects are stronger at TMO surfaces, which further makes O–O bond breaking difficult. To validate the predictions and ascertain their generalizability for TMOs, we report experimental ORR catalyst screening for 7,798 unique TMO compositions that generally exhibit activity well below that of Pt.

The oxygen reduction reaction (ORR) is the key bottleneck in the performance of low-temperature fuel cells[1–4]. The most active catalysts so far for the reaction are based on Pt group metals, but these catalysts still suffer from considerable energy losses due to a sluggish ORR[5–7]. Transition metal oxides (TMOs) constitute a rich class of materials that stand a chance of being stable under oxidizing conditions[8], but unfortunately they are found not to be nearly as active as Pt.

In this work, on the basis of density functional theory (DFT) calculations and microkinetic modelling, we identify two reasons as to why it is difficult to find TMOs with a high ORR catalytic activity. The first is that TMO surfaces consistently bind oxygen atoms more weakly than do transition metals. This makes O–O bond breaking rate-determining in a number of cases, and limits the catalytic activity relative to that of metals. The second reason is that electric field effects are stronger at TMO surfaces, which further makes O–O bond breaking difficult, in particular under acidic conditions. These two effects synergistically influence the activity of ORR on TMO surfaces.

Results

Insights from experiments. In the acidic ORR panel of Fig. 1, we show a summary of the performance of representative stable TMO catalysts for acidic ORRs published over the past 12 years (for more details, see Supplementary Figs. 1 and 2 and Supplementary Methods). In alkaline fuel cells, the stability requirements are less demanding, so it is possible to investigate many more systems for their ORR activity. Given the limited range of TMO compositions reported in the literature and the propensity for the oxygen evolution catalysis to be optimized with complex TMOs[9,10], we embarked on a large experimental ORR catalyst screening campaign. The ORR activities for 7,798 unique TMO compositions based on Mn, Ni and Fe mixed with various combinations of Ca, Mg, Y, In and La were measured after two hours of catalyst operation (to mitigate the current from transient reactions), to yield the results in the alkaline ORR panel of Fig. 1 (for more details, which include experimental procedures, see Methods and Supplementary Figs. 1 and 3). Our high-throughput experiments show optimized compositions with a current density about three times lower than that of Pt on a geometric-area basis, a relative inactivity that is only further exacerbated when the intrinsic activity due to the roughness of the TMO catalysts is considered. Our results are in agreement with those of alkaline ORR catalysts in the literature[11], which include recent results for Mn–Co oxides that show an ORR rate under alkaline conditions that is lower than that of Pt except at the highest current densities at cell voltages below 0.4 V, where the current density is typically diffusion limited[12]. The analysis shown in Fig. 1 suggests that some intrinsic limitations exist on TMOs for both acidic and alkaline ORR. Given that Pt has a large overpotential[3–5] and the inability of TMO catalysts to rival or surpass the activity of Pt at a moderate overpotential merits further investigation of any underlying universal descriptors that limit TMO catalysis of the ORR.

Calculations and modelling. In Fig. 2 we compare our calculated free energy diagram for two stable TMOs to that of the quintessential ORR catalyst, Pt (with data from Kulkarni et al.[1]). Estimates of energy barriers for the elementary steps are based on the scaling relations from Dickens et al.[13] (see below). Surface Pourbaix diagram calculations show that the stoichiometric pristine TMO surfaces are the most favourable under ORR potentials in both acid and base (Supplementary Fig. 4). Therefore, the free-energy pathways of these two TMOs are representative for both acidic and alkaline ORR conditions. The striking difference between the TMOs and Pt is the stability of adsorbed O* and the associated transition state for O–O bond breaking. Both are much less stable on the TMOs regardless of the reaction pH. This is a general phenomenon, as illustrated in

---

[1] Catalysis Theory Center, Department of Physics, Technical University of Denmark, Lyngby, Denmark. [2] Department of Chemical Engineering, Stanford University, Stanford, CA, USA. [3] Division of Engineering and Applied Science, California Institute of Technology, Pasadena, CA, USA. [4] These authors contributed equally: Hao Li, Sara Kelly. ✉e-mail: jkno@dtu.dk

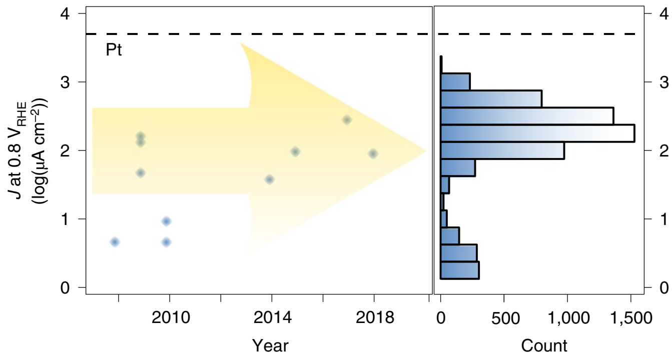

Fig. 1 | Summary of the performance of TMO catalysts. Left: the current density at 0.8 V_{RHE} for ten catalysts of the ORR in acid from the literature for which this metric is available[36–44]; each catalyst exhibits at least a 30× lower activity than that of Pt. Right: enabled by the broader range of TMOs that are stable in alkaline conditions, 7,798 complex TMOs were evaluated using high-throughput techniques, as summarized by the histogram. The dashed line is the value of pure Pt catalysts for acidic ORR[5]. Catalysts with a current density below 1 µA cm^{-2} are not shown.

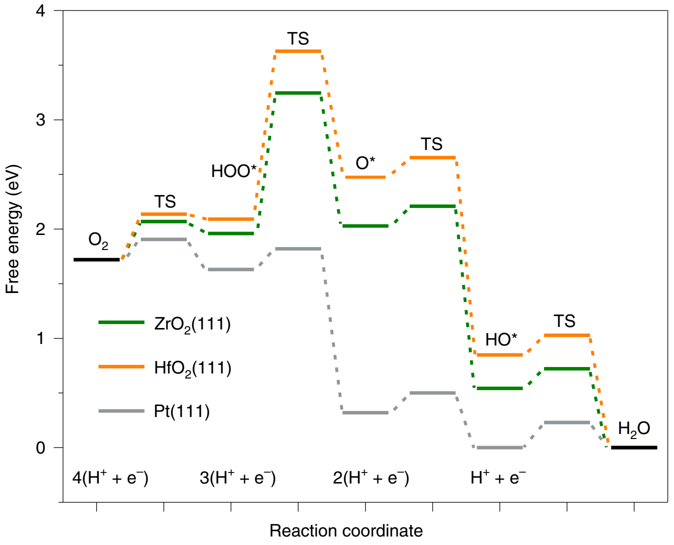

Fig. 2 | Free-energy diagram for the four-electron (4e⁻) ORR process on Pt, ZrO_2 and HfO_2(111). Surface Pourbaix diagram calculations suggest that the stoichiometric pristine surfaces of these two TMOs are favourable under ORR potentials in both acidic and alkaline conditions (Supplementary Fig. 4). $U = 0.80$ V. TS, transition state.

Fig. 3. We performed DFT calculations of the adsorption energies of ORR intermediates on more than 200 different TMOs and low- and higher-index surfaces. In Fig. 3, we collect data for the scaling relations between the adsorption energy of HOO* versus HO* and O* versus HO*. The first is universal—the same for the TMOs as for the transition metals (Fig. 3a). The latter, however, is very different for the TMOs than for the metals (Fig. 3b–d). This is one of the two key theoretical findings of this study. We note that this result is independent of whether we include a Hubbard *U* in the calculations or not. We return to the reason for the unstable O adsorption on the TMOs below.

The generally weak O bonding on the TMOs directly translates into a high barrier for O–O bond breaking, due to the scaling of the barrier with $G_{O*} - G_{HOO*}$, which we derived on the basis of previously published data for the reverse reaction on TMOs (Fig. 3e)[13]. The weak bonding of oxygen (large $G_{O*} - G_{HO*}$ or because of the universal HO versus HOO scaling, large $G_{O*} - G_{HOO*}$) results in larger barriers for the O–O bond breaking. All of these are borne out in the kinetic model of ORR shown in Fig. 4. Here, the rates of ORR are solved as a function of the HO adsorption energy using the steady-state assumption. The kinetic model is based on the scaling relations and, as all adsorption energies and transition-state energies scale, a single descriptor is sufficient. The kinetic model is developed in Hansen et al.[14] and Kelly et al.[15].

For the transition metals there are generally two important steps that determine the rate—the adsorption of O_2 and the removal of HO* from the surface[14,16]. This leads to a volcano-shaped dependence (Fig. 4a) in which metals with HO adsorption energies on the left leg (strong HO adsorption) are limited by too strong a HO bonding that leaves no sites free for catalysis. This includes Pt (ref. [17]). The metals on the right leg, however, are characterized by a rate limited by O_2 activation because weak HO adsorption correlates with a high barrier for O_2 activation[15].

The O–O bond breaking is not rate-determining on transition metals, because of the very stable O*. This is different for the TMOs. Here, the weak interaction with O means that the transition state for O–O bond breaking becomes high and this step becomes rate-determining for many TMOs. To illustrate this switch, we include an analysis of the rate assuming that HO* coverage, O_2 protonation or O–O bond breaking are rate-limiting, which shows clearly that O–O bond breaking affects the overall rate of ORR on TMOs but not on metals (Fig. 4b,c). For the TMOs (as for the metals), we see a surface-structure dependence of the scaling relations, which is reflected in the rate volcanoes in Fig. 4. A similar structure dependence has been observed in OER catalysis and it has been shown to reflect differences in the surface electronic structure for different oxygen coordination environments[18]. Owing to the complexity in analysing the local oxygen density of various TMO surfaces, our current work qualitatively classifies the structures into low- and higher-index TMOs. On higher-index TMO surfaces, the volcano is qualitatively different from that of transition metals. Notably, the maximum is shifted towards more strongly bonding surfaces and, most importantly, the maximum rate is considerably less than that for transition metals—or, equivalently, the minimum overpotential at a given current density is increased significantly (Fig. 4c). We suggest that this is an important factor in explaining the observations in Fig. 1. The low-index TMOs also have a volcano shifted towards more strongly bonding surfaces, but with the maximum rate closer to that of transition metals (Fig. 4b). Owing to the steeper volcano right leg, the search for high-activity low-index TMOs is also narrowed. We note that, of the binary oxides in our high-throughput screening, MnO_x exhibits the highest activity (Supplementary Fig. 3), in excellent agreement with Fig. 4b. In addition, all of the catalyst compositions in the top 10% of current densities at 0.8 V_{RHE} (RHE, reversible hydrogen electrode) (Fig. 1) in our high-throughput experiments contain Mn, often in combination with Ni.

Modelling pH with an electric field. The analysis above suggests that most TMO surfaces are considerably less active than the most active transition metals, and even the best low-index surfaces are only comparable with Pt. We now turn to an additional effect that can contribute to an increase of the overpotential of even the low-index TMOs relative to that attainable with metals. Recent studies showed that electric field effects can explain the pH dependencies of weakly binding metal ORR catalysts[15,19]. Although it is difficult to measure the exact magnitude of the electric field under experimental conditions, we can expect it to increase with increasing absolute potential. The field interacts with intermediates and transition states with a substantial dipole moment and/or

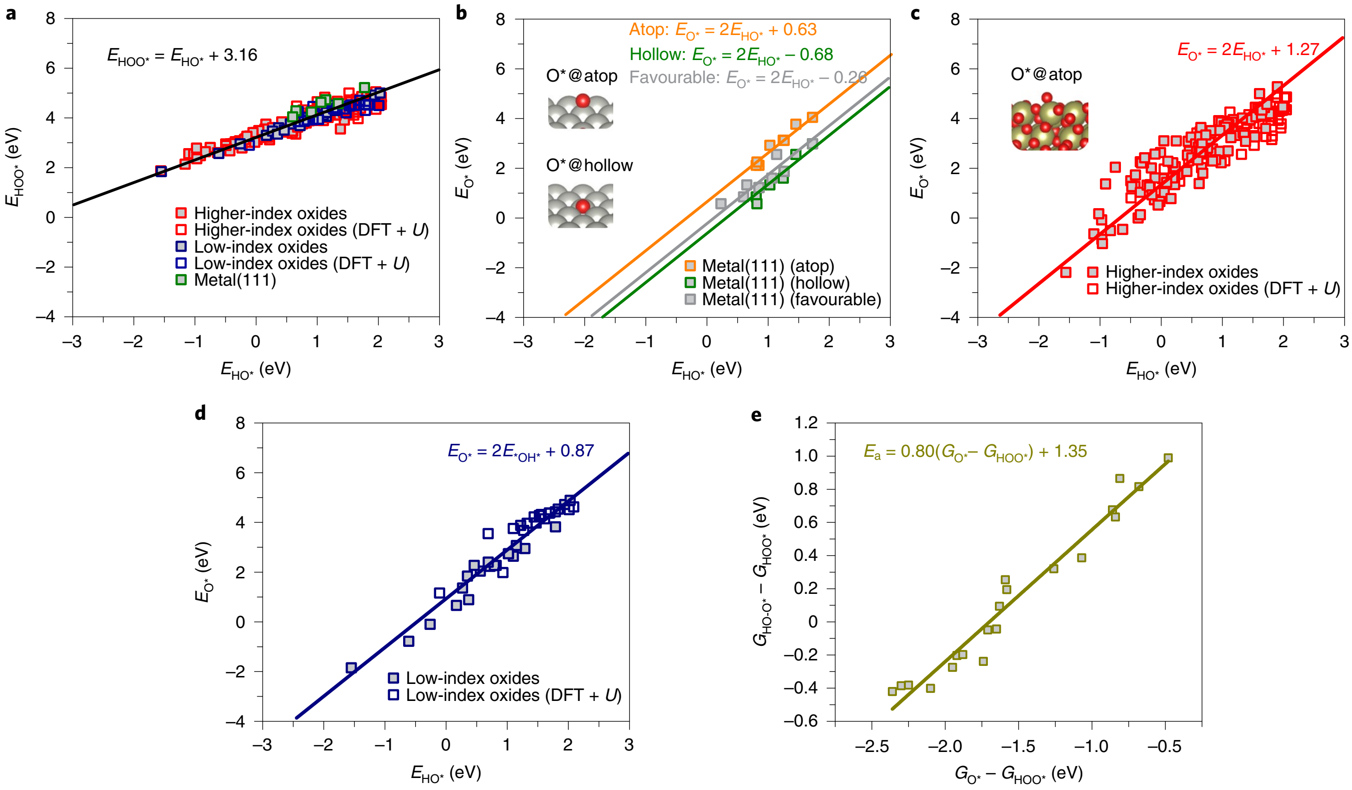

Fig. 3 | Linear scaling relations that determine the ORR activities. a, The universal scaling relation of E_{HO*} versus E_{HOO*}. **b**, E_{HO*} versus E_{O*} scaling relation on transition metal (111) surfaces. **c**, E_{HO*} versus E_{O*} scaling relation on higher-index ($h^2+k^2+l^2>1$) TMO surfaces. **d**, E_{HO*} versus E_{O*} scaling relation on low-index ($h^2+k^2+l^2=1$) TMO surfaces. **e**, Transition-state energy ($G_{HO\text{-}O*} - G_{HOO*}$) versus ΔG ($G_{O*} - G_{HOO*}$) at $U=0$ V (ref. [13]). All the energies are relative to those of H_2 and H_2O. DFT + U represents the TMO systems calculated with strong on-site Coulomb interaction corrections for localized electrons. Red, grey and yellow spheres represent O, the element of the transition metal (111) surfaces and the element of the TMO surfaces, respectively.

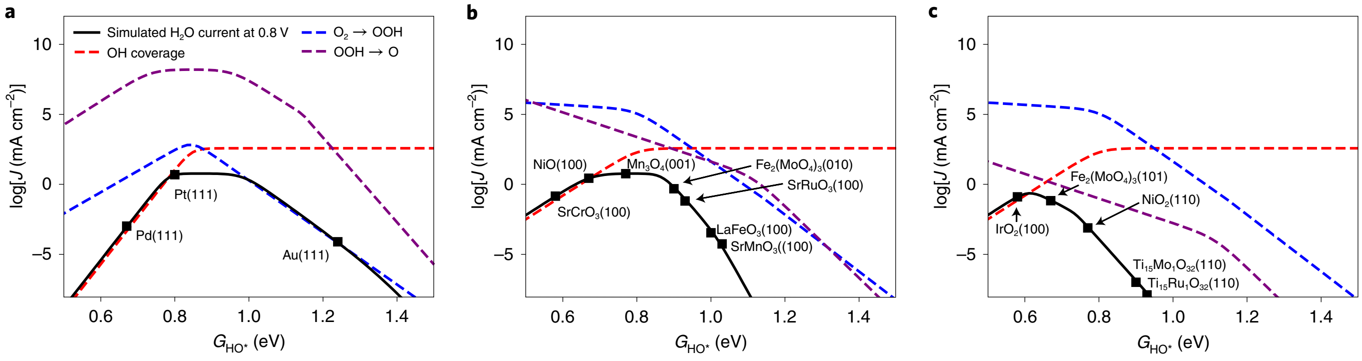

Fig. 4 | Kinetic volcano models for the 4e⁻ ORR process at 0.8 V_{RHE}. a, Volcano activity model for transition metal surfaces. **b**,**c**, Volcano activity models for low-index (**b**) and higher-index (**c**) TMO surfaces. Dashed lines indicate the activity of the 4e⁻ ORR as solved by rate-determining-step analysis with the rate limited by O_2 protonation (blue), HOO* protonation and splitting (purple) and HO* coverage (red).

polarizability. The oxygen species of interest here generally have positive dipole moments, which means they are stabilized at negative fields and destabilized at positive fields. As has been shown in previous studies, an electric field can be approximated to be linearly dependent on an absolute potential, such as the standard hydrogen potential[15,20,21]. This means that changes in adsorbate energy due to an electric field will appear to be pH dependent on an RHE scale, which differs from the standard hydrogen potential only by pH. Figure 5a–c shows examples of how metal and TMO surfaces respond to different electric fields (with the metal data from Kelly et al.[15]. and other details shown in Supplementary Methods). Notably, we can see a much more significant response to the electric field effects on the TMO surfaces as compared with that of metals, with a more significant tuning of the adsorbate (especially adsorbed O) bonding strength at the surface. Figure 5d–f shows the pH effect on the volcanos modelled with the electric field effects (for the computational details, see Supplementary Methods). In an acidic solution (that is, a more positive electric field), the effect on the activity volcano of the transition metals is minor (Fig. 5a). In contrast, the volcanos are

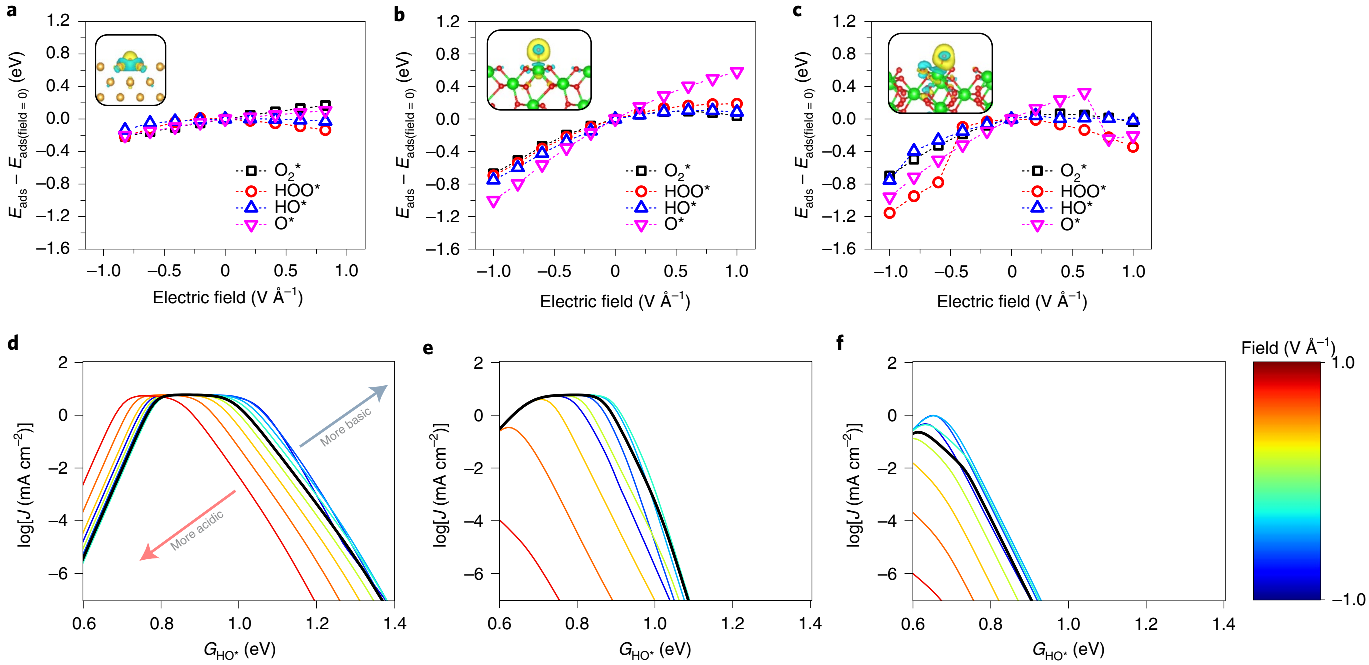

Fig. 5 | Electric field effects and pH-dependent kinetic volcano models. a–c, Electric field effects on the adsorbate bindings on Au(100) (**a**)[15], ZrO_2(100) (**b**) and ZrO_2(111) (**c**). Red, yellow and green spheres represent O, Au and Zr, respectively. **d**, Volcano activity models for transition metal surfaces. Insets: the charge density difference induced by the adsorption of atomic oxygen. The yellow and teal colours in the isosurfaces represent electron charge gain and loss, respectively. **e**,**f**, Volcano activity models for low-index (**e**) and higher-index (**f**) TMO surfaces. The higher and lower electric fields represent more acidic and basic conditions, respectively.

left- and down shifted with a general decrease in the maximum rates for both the low- and higher-index TMOs at more acidic conditions (Fig. 5b,c). The effect is stronger on the TMOs than on the metals because of the generally larger surface dipole and polarizability, which originate from the fact that on TMO surfaces, O and other adsorbates can, in most instances, only adsorb in an atop site, whereas they can find a more stable high-coordination adsorption site on the transition meal surfaces. These are in excellent agreement with previous experiments that there is a pH dependency of the ORR performance on TMO catalysts[22–25], in which a lower pH leads to a worse ORR performance. As there is little information about the potential of zero charge of TMO surfaces, and about the capacitances at and above these surfaces, we cannot comment on the absolute magnitude of the shifts due to field effects on these TMOs. The field effects can therefore only be viewed as qualitative at the moment, recognizing that an increasing pH will lead to a decreasing field at a constant RHE potential.

All in all, electric field effects can provide the second reason why TMOs have an intrinsically limited performance for 4e$^-$ ORR in acid. Clearly, the present model, at least qualitatively, also explains why TMOs seem to be better in an alkaline than an acidic solution. We note that our model suggests that TMOs are more active for 2e$^-$ ORR in both acid and base due to the unchanged HO versus HOO scaling relation (Fig. 3a and Supplementary Fig. 5), in good agreement with many experimental observations[26–28]. The best TMO surfaces (based on Mn and Ni) in our theoretical and experimental analysis approach an activity close to that of Pt. However, they still suffer from the fact that they are most active in a base and that they have a relatively high 2e$^-$ selectivity (Supplementary Fig. 5), both effects being understandable in our model.

Discussion

We finally turn to the question of the origin of the weaker O bonding and stronger field effects found at TMO surfaces. First, we focus on the weaker O bonding. As illustrated in Fig. 2b, the scaling relation of E_{O^*} versus E_{HO^*} on metals is quite specific to the adsorption site as O* has a different binding mode compared with those of HO* and HOO*. On close-packed transition metals, O adsorbs in a three-fold site, whereas HO and HOO prefer two- or one-fold sites. If, instead of plotting the E_{O^*} versus E_{HO^*} scaling relation with O in the preferred site, we force the O to be adsorbed in an on-top site, a significant upshift in the HO versus O scaling line is observed (Fig. 2b). This is the main origin of the effect. For TMOs, the O atoms generally adsorb in one-fold sites on both the higher- and low-index surfaces and do not have the possibility of a higher metal coordination number as on the metal surfaces. This observation was first made by the Rossmeisl group for single-atom metal-doped nitrogen–carbon systems[29], with a scaling intercept close to that of our low-index TMO surfaces. The high field effects for O adsorption energies on TMO surfaces have the same geometrical origin. An O atom that adsorbs on top of a metal atom is further away from the surface and thus gives a large adsorption-induced dipole moment. On metallic surfaces, an adsorbed O atom is physically closer to the catalyst surface, which results in considerably more spatial overlap of the O* and metal electron density. The workfunction changes on atomic O adsorption ($\Delta WF = WF_{O^*} - WF_*$, where WF_{O^*} and WF_* are the workfunctions of the system with and without adsorbed O*, respectively) on Au(100), ZrO_2(100) and ZrO_2(111) are 0.20, 2.81 and 2.33 eV, respectively, which indicates a much larger dipole induced by the on-top site adsorption. All of these are illustrated by the insets in Fig. 5a–c.

Consequently, the weak O binding and large field effects of TMO catalysts (compared with those of metals) both appear to arise from the single O–TM bond on O-saturated TMO surfaces. This leads to a weak bond and a large surface dipole moment compared with those of transition metal surfaces, where the O atoms can bind with a higher metal coordination number.

The analysis above suggests that a good strategy to discover more ORR-active TMOs could be to search for exceptions to the high HO versus O scaling that we generally see for TMOs. One avenue is to consider stable TMOs with a higher coordination O adsorption, as argued above. This could be defect sites or lattice oxygen for weak-bonding TMOs. Also, to find ORR electrocatalysts that are better than Pt, we need to find ways to significantly shift the scaling of not just the O adsorption energy and O–O bond breaking barrier, but also the barrier(s) for O_2 activation to form adsorbed HOO. This will most probably require new or unexplored multifunctional active sites.

Methods

High-throughput synthesis. High-throughput synthesis and electrochemical characterization proceeded using inkjet printing and calcination[9] followed by serial experimentation with a scanning droplet cell[30] and parallel accelerated ageing[31] techniques, with each process described in detailed in the respective citation. Considering a set of 6 cation elements, there are 2,112 unique compositions that contain 1, 2, 3 or 4 cation elements with 10 at% intervals[9]. Synthesis of this set of compositions was performed for 7 unique sets of 6 cation elements: Mg–Ca–La–Ni–Mn–Fe, Mg–Ca–Ni–Mn–Fe–Y, Ca–In–La–Ni–Mn–Y, In–La–Ni–Mn–Fe–Y, Mg–Ca–In–Ni–Mn–Fe, Mg–Ca–In–La–Fe–Y and Mg–In–La–Ni–Mn–Y. The 2,112 unique compositions for each set were deposited as a grid of $1\times 1\,\mathrm{mm}^2$ samples, each containing approximately 4 nmol cation elements, on fluorine-doped tin oxide (FTO Tec 7)-coated glass and calcined in a tube furnace with O_2 (300 torr) at 450 °C for 10 h.

Electrochemical measurements. Electrochemical measurements were performed in three-electrode configuration with a Ag/AgCl reference electrode and potentials adjusted to V_{RHE} using a pH of 14. All the measurements were performed in 1 M NaOH aqueous electrolyte saturated with O_2 via bubbling with ~1 atm O_2 gas. The sequence of electrochemical experiments was eight cyclic voltammograms (CV) from 1.23 to 0.63 V versus RHE at a sweep rate of $0.25\,\mathrm{V\,s^{-1}}$, chronoamperometry at 0.63 V versus RHE for 4 s, with the current over the final 1 s averaged and divided by the $1\,\mathrm{mm}^2$ catalyst area to produce the geometric current density, chronoamperometry of the entire library at 0.8 V versus RHE for 2 h under flowing electrolyte, three CV cycles from 1.23 to 0.63 V versus RHE at a sweep rate of $0.25\,\mathrm{V\,s^{-1}}$, a single CV at $0.05\,\mathrm{V\,s^{-1}}$ over the same potential range and a 4 s chronoamperometry measurement at 0.63 V versus RHE. The cathodic and anodic sweeps of the final CV were averaged to mitigate the influence from capacitive currents, and the resulting signal was evaluated at the desired potential, 0.8 V versus RHE, to obtain the current densities for Fig. 1 and Supplementary Fig. 1. Additional experimental details and discussions can be found in Supplementary Discussion.

Computational methods. DFT calculations were performed using the generalized gradient approximation method with the revised Perdew−Burke−Ernzerhof functional to describe electronic exchange and correlations[32,33]. A projector augmented-wave method was used to describe the core electrons[34]. Valence electrons were described by expanding the Kohn–Sham wavefunctions in a plane-wave basis set[35], with a cutoff of at least 400 eV. The complete computational and modelling details can be found in Supplementary Methods.

Data availability

The experimental data are available at https://data.caltech.edu/records/1632 (https://doi.org/10.22002/D1.1632). The computational data, which include the O, HO and HOO binding energies, the free energies of $4e^-$ ORR, the optimized atomic coordinates and the scripts for structure modelling, are available at https://github.com/cattheory-oxides/data. All the data are available from the authors upon reasonable request.

Received: 7 October 2020; Accepted: 19 April 2021;
Published online: 24 May 2021

References

1. Kulkarni, A., Siahrostami, S., Patel, A. & Nørskov, J. K. Understanding catalytic activity trends in the oxygen reduction reaction. *Chem. Rev.* **118**, 2302–2312 (2018).
2. Gasteiger, H. A. & Markovic, N. M. Just a dream or future reality? *Science* **324**, 48–49 (2009).
3. Debe, M. K. Electrocatalyst approaches and challenges for automotive fuel cells. *Nature* **486**, 43–51 (2012).
4. Marković, N. M., Schmidt, T. J., Stamenković, V. & Ross, P. N. Oxygen reduction reaction on Pt and Pt bimetallic surfaces: a selective review. *Fuel Cells* **1**, 105–116 (2001).
5. Escudero-Escribano, M. et al. Tuning the activity of Pt alloy electrocatalysts by means of the lanthanide contraction. *Science* **352**, 73–76 (2016).
6. Greeley, J. et al. Alloys of platinum and early transition metals as oxygen reduction electrocatalysts. *Nat. Chem.* **1**, 552–556 (2009).
7. Sakong, S. & Groß, A. Water structures on a Pt(111) electrode from ab initio molecular dynamic simulations for a variety of electrochemical conditions. *Phys. Chem. Chem. Phys.* **22**, 10431–10437 (2020).
8. Ota, K. I. et al. Development of group 4 and 5 metal oxide-based cathodes for polymer electrolyte fuel cell. *J. Power Sources* **196**, 5256–5263 (2011).
9. Stein, H. S. et al. Functional mapping reveals mechanistic clusters for OER catalysis across (Cu–Mn–Ta–Co–Sn–Fe)O_x composition and pH space. *Mater. Horiz.* **6**, 1251–1258 (2019).
10. Haber, J. A. et al. Discovering Ce-rich oxygen evolution catalysts, from high throughput screening to water electrolysis. *Energy Environ. Sci.* **7**, 682–688 (2014).
11. Wang, Y., Li, J. & Wei, Z. Transition-metal-oxide-based catalysts for the oxygen reduction reaction. *J. Mater. Chem. A* **6**, 8194–8209 (2018).
12. Wang, Y. et al. Synergistic Mn–Co catalyst outperforms Pt on high-rate oxygen reduction for alkaline polymer electrolyte fuel cells. *Nat. Commun.* **10**, 1506 (2019).
13. Dickens, C. F., Kirk, C. & Nørskov, J. K. Insights into the electrochemical oxygen evolution reaction with ab initio calculations and microkinetic modeling: beyond the limiting potential volcano. *J. Phys. Chem. C.* **123**, 18960–18977 (2019).
14. Hansen, H. A., Viswanathan, V. & Nørskov, J. K. Unifying kinetic and thermodynamic analysis of $2e^-$ and $4e^-$ reduction of oxygen on metal surfaces. *J. Phys. Chem. C* **118**, 6706–6718 (2014).
15. Kelly, S. R., Kirk, C., Chan, K. & Nørskov, J. K. Electric field effects in oxygen reduction kinetics: rationalizing pH dependence at the Pt(111), Au(111), and Au(100) electrodes. *J. Phys. Chem. C* **124**, 14581–14591 (2020).
16. Nørskov, J. K. et al. Origin of the overpotential for oxygen reduction at a fuel-cell cathode. *J. Phys. Chem. B* **108**, 17886–17892 (2004).
17. Wang, J. X., Markovic, N. M. & Adzic, R. R. Kinetic analysis of oxygen reduction on Pt(111) in acid solutions: intrinsic kinetic parameters and anion adsorption effects. *J. Phys. Chem. B* **108**, 4127–4133 (2004).
18. Dickens, C. F., Montoya, J. H., Kulkarni, A. R., Bajdich, M. & Nørskov, J. K. An electronic structure descriptor for oxygen reactivity at metal and metal–oxide surfaces. *Surf. Sci.* **681**, 122–129 (2019).
19. Duan, Z. & Henkelman, G. Theoretical resolution of the exceptional oxygen reduction activity of Au(100) in alkaline media. *ACS Catal.* **9**, 5567–5573 (2019).
20. Chen, L. D., Urushihara, M., Chan, K. & Nørskov, J. K. Electric field effects in electrochemical CO_2 reduction. *ACS Catal.* **6**, 7133–7139 (2016).
21. Lamoureux, P. S., Singh, A. R. & Chan, K. pH effects on hydrogen evolution and oxidation over Pt(111): insights from first-principles. *ACS Catal.* **9**, 6194–6201 (2019).
22. Mittermeier, T., Madkikar, P., Wang, X., Gasteiger, H. A. & Piana, M. ZrO_2 based oxygen reduction catalysts for PEMFCs: towards a better understanding. *J. Electrochem. Soc.* **163**, F1543 (2016).
23. Jung, J. W., Kim, G. Y., Lee, N. W. & Ryu, W. H. Low-temperature synthesis of tetragonal phase of hafnium oxide using polymer-blended nanofiber precursor. *Appl. Surf. Sci.* **533**, 147496 (2020).
24. Matsui, T. et al. Catalytic activities for oxygen reduction reaction of group 4 and 5 transition metal oxide-based compounds in alkaline solution. *220th ECS Meeting Abstracts 2011-02* 293 (Electrochemical Society, 2011).
25. Hu, S. *Corrosion-Resistant Transition Metal Oxides and Oxynitrides Evaluated as Potential Non-Noble Metal Electrocatalysts for the Oxygen Reduction Reaction*. PhD thesis, State Univ. of New York at Stony Brook (2015).
26. Carneiro, J. F., Paulo, M. J., Siaj, M., Tavares, A. C. & Lanza, M. R. V. Zirconia on reduced graphene oxide Sheets: synergistic catalyst with high selectivity for H_2O_2 electrogeneration. *ChemElectroChem* **4**, 508–513 (2017).
27. Carneiro, J. F., Paulo, M. J., Siaj, M., Tavares, A. C. & Lanza, M. R. V. Nb_2O_5 nanoparticles supported on reduced graphene oxide sheets as electrocatalyst for the H_2O_2 electrogeneration. *J. Catal.* **332**, 51–61 (2015).
28. Barros, W. R. P. et al. Oxygen reduction to hydrogen peroxide on Fe_3O_4 nanoparticles supported on Printex carbon and graphene. *Electrochim. Acta* **162**, 263–270 (2015).
29. Wan, H., Jensen, A. W., Escudero-Escribano, M. & Rossmeisl, J. Insights in the oxygen reduction reaction: from metallic electrocatalysts to diporphyrins. *ACS Catal.* **10**, 5979–5989 (2020).
30. Gregoire, J. M., Xiang, C., Liu, X., Marcin, M. & Jin, J. Scanning droplet cell for high throughput electrochemical and photoelectrochemical measurements. *Rev. Sci. Instrum.* **84**, 024102 (2013).
31. Jones, R. J. R. et al. Parallel electrochemical treatment system and application for identifying acid-stable oxygen evolution electrocatalysts. *ACS Comb. Sci.* **17**, 71–75 (2015).
32. Perdew, J. P., Burke, K. & Ernzerhof, M. Generalized gradient approximation made simple. *Phys. Rev. Lett.* **77**, 3865–3868 (1996).

33. Hammer, B., Hansen, L. B. & Nørskov, J. K. Improved adsorption energetics within density-functional theory using revised Perdew–Burke–Ernzerhof functionals. *Phys. Rev. B* **59**, 7413 (1999).
34. Blöchl, P. E. Projector augmented-wave method. *Phys. Rev. B* **50**, 17953–17979 (1994).
35. Kohn, W. & Sham, L. J. Self-consistent equations including exchange and correlation effects. *Phys. Rev.* **140**, A1133 (1965).
36. Ishihara, A., Shibata, Y., Mitsushima, S. & Ota, K. Partially oxidized tantalum carbonitrides as a new nonplatinum cathode for PEFC−1−. *J. Electrochem. Soc.* **155**, B400–B406 (2008).
37. Nam, K. D., Ishihara, A., Matsuzawa, K., Mitsushima, S. & Ota, K. I. Partially oxidized niobium carbonitride as non-platinum cathode for PEFC. *Electrochem. Solid-State Lett.* **12**, B158 (2009).
38. Takasu, Y., Oohori, K., Yoshinaga, N. & Sugimoto, W. An examination of the oxygen reduction reaction on RuO_2-based oxide coatings formed on titanium substrates. *Catal. Today* **146**, 248–252 (2009).
39. Liu, Y., Ishihara, A., Mitsushima, S. & Ota, K. Influence of sputtering power on oxygen reduction reaction activity of zirconium oxides prepared by radio frequency reactive sputtering. *Electrochim. Acta* **55**, 1239–1244 (2010).
40. Takasu, Y., Suzuki, M., Yang, H., Ohashi, T. & Sugimoto, W. Oxygen reduction characteristics of several valve metal oxide electrodes in $HClO_4$ solution. *Electrochim. Acta* **55**, 8220–8229 (2010).
41. Seo, J., Cha, D., Takanabe, K., Kubota, J. & Domen, K. Particle size dependence on oxygen reduction reaction activity of electrodeposited TaO_x catalysts in acidic media. *Phys. Chem. Chem. Phys.* **16**, 895–898 (2014).
42. Ishihara, A. et al. Synthesis of nano-TaO_x oxygen reduction reaction catalysts on multi-walled carbon nanotubes connected via a decomposition of oxy-tantalum phthalocyanine. *Phys. Chem. Chem. Phys.* **17**, 7643–7647 (2015).
43. Tominaka, S., Ishihara, A., Nagai, T. & Ota, K. I. Noncrystalline titanium oxide catalysts for electrochemical oxygen reduction reactions. *ACS Omega* **2**, 5209–5214 (2017).
44. Chisaka, M. Creation of oxygen reduction reaction active sites on titanium oxynitride without increasing the nitrogen doping level. *Phys. Chem. Chem. Phys.* **20**, 15613–15617 (2018).

Acknowledgements

We thank I. Chorkendorff, Y. Zheng (Technical University of Denmark), T. F. Jaramillo (Stanford University) and J. H. Montoya (Toyota Research Institute) for all the helpful discussions. This work was supported by the Toyota Research Institute through the Accelerated Materials Design and Discovery program.

Author contributions

H.L., S.K., J.M.G. and J.K.N. designed the study and wrote the paper. H.L., S.K., Z.W., M.A., G.T.K.K.G., C.S.A. and S.V. conducted the DFT calculations, data analysis, and microkinetic modelling. D.G., Y.W., J.A.H. and J.M.G. performed the high-throughput experiments.

Competing interests

The authors declare no competing interests.

Additional information

Supplementary information The online version contains supplementary material available at https://doi.org/10.1038/s41929-021-00618-w.

Correspondence and requests for materials should be addressed to J.K.N.

Peer review information *Nature Catalysis* thanks Guofeng Wang and the other, anonymous, reviewer(s) for their contribution to the peer review of this work.